Supplementary Material (ESI) for Chemical Communications

Electronic Supplementary Information

for

pH-controllable Drug Release Using Hydrogel Encapsulated Meosporous Silica

S.-W. Song, K. Hidajat, and S. Kawi

Department of Chemical and Biomolecular Engineering, National University of Singapore, 4 Engineering Drive 4, Singapore 119260.

Materials and Methods

Synthesis of SBA-15 materials. Ethanol-extracted SBA-15 (ES-15) was prepared according to the procedure reported by Zhao et al. [1] using Pluronic 123 triblock polymer [$(EO)_{20}(PO)_{70}(EO)_{20}$, M_{av} = 5800, Aldrich, USA] as a structure directing agent and tetraethylorthosilicate (TEOS, Aldrich, USA) as the silica source. The molar composition of the mixture was 1 SiO_2: 0.017 P_{123}: 2.9 HCl: 202.6 H_2O. The mixture was stirred to react at 40ºC for 24 hrs followed by hydrothermal treatment at 110ºC for 48 hrs under static condition in a Teflon-lined autoclave. After reaction, the resulting white solid was washed with deionized water, filtered and dried at 60ºC overnight. The surfactant template was removed by refluxing 2 g of sample with 100 cm^3 ethanol for 24 hrs. The material was filtered, washed with ethanol and deionized water alternately for several times, and then dried at 60ºC.

Amine-functionalized SBA-15 prepared by one-pot synthesis (OPS-15) was carried out using the same procedure as that used in the synthesis of ethanol-extracted SBA-15, except that functional agent 3-aminopropyltriethoxysilane (APTES, Sigma-Aldrich, USA) was introduced together with TEOS. The molar composition of

the mixture was 1 TEOS: 0.05 APTES: 0.017 P_{123}: 2.9 HCl: 202.6 H_2O. The hydrothermal treatment for the material was carried out at 120ºC for 48 hrs under static conditions.

Amine-functionalized SBA-15 prepared by post-synthesis (PS-15) was carried out using the same procedure as that used in the synthesis of ethanol-extracted SBA-15, except that the temperature of hydrothermal treatment for the material was at 120ºC for 48 hrs under static conditions and the organic template was removed by calcination. Then 1.0 g of the calcined purely-siliceous SBA-15 was treated with 4mM of APTES in 30 ml of 1, 4 dioxane (99%, Sigma-Aldrich, USA) under reflux for 24 hrs. The resultant white solid was filtered off, washed with diethyl ether (3×20 cm^3, Sigma-Aldrich, USA) and dried under vacuum.

Characterization methods. Nitrogen adsorption/desorption measurements were conducted using Quantachrome Autosorb-1 by N_2 physisorption at 77 K. The BET specific surface areas of the samples were calculated in the range of relative pressures between 0.05 and 0.30. The pore size distributions were calculated from the adsorption branch of isotherm using Barrett-Joyner-Halenda (BJH) method. The total pore volume was determined from the adsorption branch of the N_2 isotherm at P/P_0 = 0.95. Zeta potential measurements were performed using a ZetaPlus zeta potential analyzer (Brookhaven Instruments). FT-IR spectra were collected using a Shimadzu FTIR-8700 with a resolution of 2 cm^{-1}. 10 mg of sample was pressed (under a pressure of 1 ton/cm^2 for 10 sec) into a self-supported wafer 16 mm in diameter. Prior to analysis, the wafer was treated in an in-situ quartz cell equipped with CaF_2 windows under vacuum ($<10^{-5}$ mbar). X-ray photoelectron spectroscopy (XPS) was performed on Kratos AXIS HIS instrument to characterize the surface species. An Mg Kα X-ray source (hν = 1253.6) with analyzer pass energy of 40 eV was operated at 10 mA and 15 kV. All experiments presented here were performed in an ultrahigh vacuum (UHV) chamber with a base pressure of less than 10^{-9} Torr. In all cases, the binding energy of the C1s core levels (284.6 eV) was used as an internal standard to distinguish between band-bending and chemical shift. The morphologies of the powder samples were visually observed using field emission scanning electron

microscopy (FESEM, JEOL JSM-6700F). Thermal gravimetric analysis (TGA) was performed using a Shimadzu DTG-60 simultaneous DTA-TG analyzer. The cytotoxicity of SBA-15 materials was evaluated using 3T3 mouse fibroblasts and 3-[4,5-dimethylthiazol-2-yl]-2,5-diphenyltetrazolium bromide thiazolyl blue (MTT) assay, and the cell viability was expressed as % of the corresponding control values.

Results

N_2 adsorption/desorption analysis. Fig. S1 gives the N_2 adsorption/desorption isotherms and pore size distributions of unfunctionalized SBA-15 (ES-15), amine-functionalized SBA-15 prepared by one-pot synthesis (OPS-15) and amine-functionalized SBA-15 prepared by post synthesis (PS-15). The three samples have similar pore size, but in comparison with ES-15 and OPS-15, PS-15 has the smallest surface area.

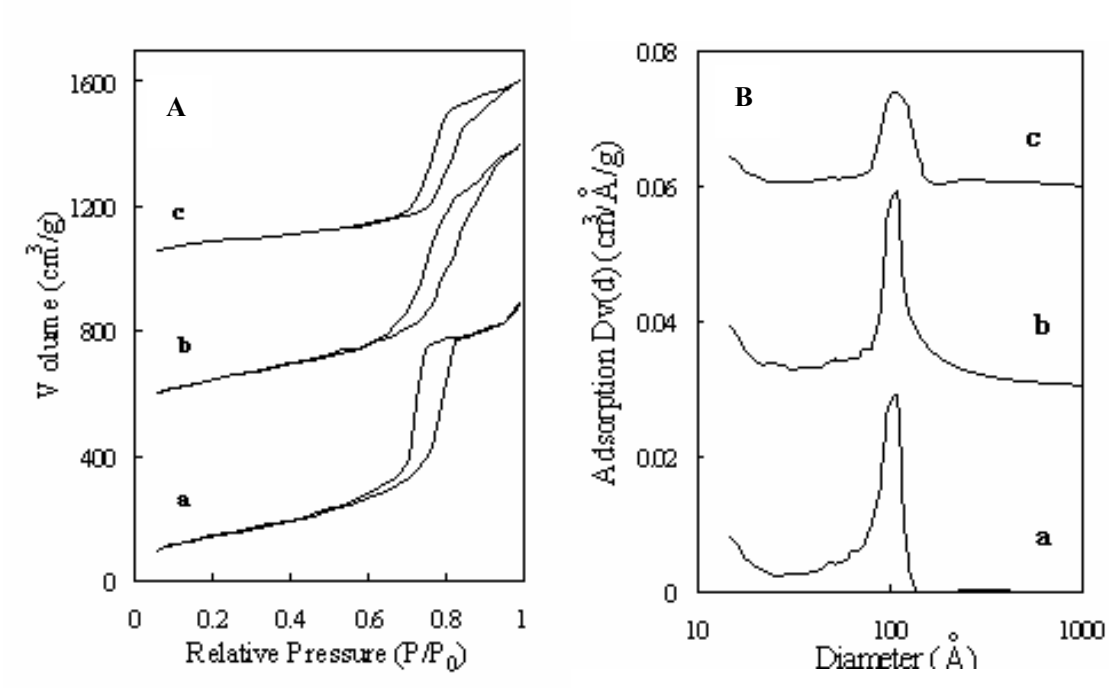

Fig. S1 (A) Nitrogen adsorption/desorption isotherms and (B) Pore size distributions of: a- ES-15; b- OPS-15 and c- PS-15. (The isotherms are offset vertically by 500 and 1000 cm^3/g for b and c respectively. And the pore size distribution curves are offset vertically by 0.03 and 0.06 $cm^3/Å/g$ for b and c, respectively.)

FTIR spectra of SBA-15 materials. Fig. S2 shows the FTIR spectra of SBA-15 samples investigated in this study. Spectrum **a** is related to the ethanol-extracted pure SBA-15, which shows the well-known IR absorption bands due to the stretching vibrational mode of surface silanol groups in the range of 3740-3500 cm^{-1} [2,3]. In spectrum **b,** which is related to functionalized SBA-15 prepared by one-pot synthesis (OPS-15), in addition to the broad band located at 3500 - 3000 cm^{-1} characterizing surface hydroxyl groups, a new infrared absorption band assigned to NH_2 asymmetric bending is observed at 1602 cm^{-1} [4]. This result shows that the surface has been successfully functionalized. For spectrum **c**, which corresponds to functionalized SBA-15 prepared by post-synthesis (PS-15), a new band assigned to NH_2 bending appears at 1595 cm^{-1} and two new bands assigned to CH_2 stretching appear at 2935 and 2867 cm^{-1} due to the methyl groups introduced during silylation. The broad band of silanol groups disappeared due to the condensation reaction during the calcination of SBA-15 and the consumption of some silanol groups as the anchoring site during functionalization. The disappearance of these silanol groups and the presence of more methyl groups on PS-15 surface make the material more hydrophobic, resulting in the agglomeration of sample powders floating on the aqueous surface of hydrophilic PAA solution. Hence PS-15 could not be encapsulated with PAA.

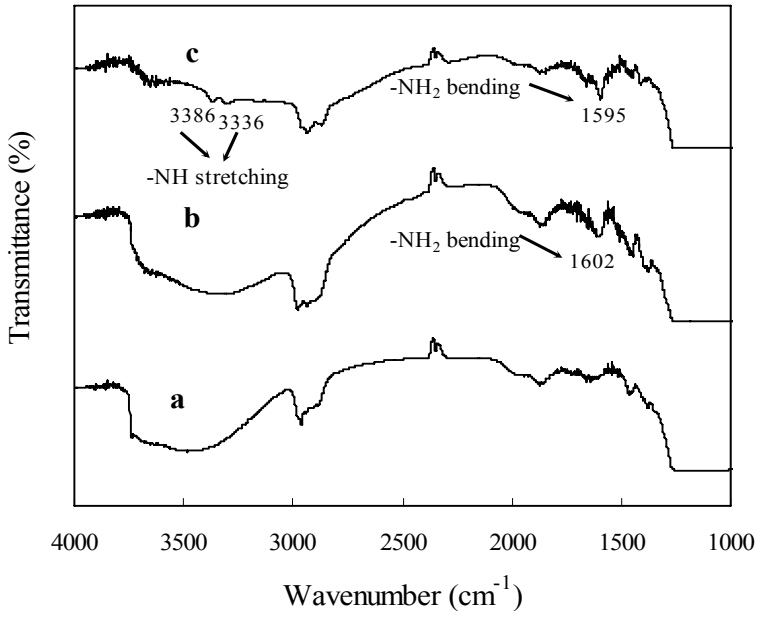

Fig. S2 FTIR spectra of: a - ES-15; b – OPS-15; c – PS-15.

ζ potential of SBA materials. Fig. S3 shows the ζ potential as a function of pH value for unfunctionalized SBA-15 (ES-15), amine-functionalized SBA-15 prepared by one-pot synthesis (OPS-15) and amine-functionalized SBA-15 prepared by post synthesis (PS-15). The ζ potential of pure silica SBA-15 is positive only at pH value below 3.5, as surface silanol groups (Si-OH) tend to lose a proton and form species ($Si\text{-}O^-$). However, in the case of amine-functionalized SBA-15, only a small amount of amine groups introduced has remarkably altered the surface charge of SBA-15. Due to the dissociation of the surface amine groups, the ζ potentials of amine-functionalized SBA-15 is positive at the pH value below around 6.7 (OPS-15) or 7.4 (PS-15). Therefore, negatively charged PAA can not be assembled onto unfunctionalized SBA-15 (ES-15) due to electrostatic repulsion.

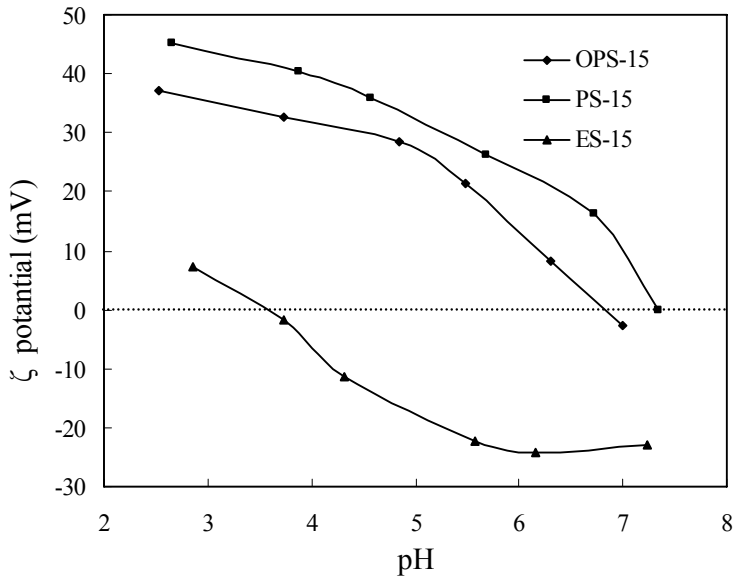

Fig. S3 ζ potential of SBA-15 samples as a function of pH value.

SEM images. Fig. S4 shows the FESEM images of ES-15 and OPS-15 before and after being coated with PAA. During the encapsulation process of both ES-15 and OPS-15, it has been observed that the powders were well dispersed in the PAA solution. After encapsulation, the powders were then washed twice with deionized water to remove the remaining polymers. However, the FESEM images of the two sample powders after encapsulation show a big difference. For ES-15, the shapes and sizes of the powders remains unchanged, suggesting that the powders could not be successfully coated with PAA. However, after OPS-15 was encapsulated with PAA, it can be clearly observed that the powders seem to stick together by polymers to form larger particles.

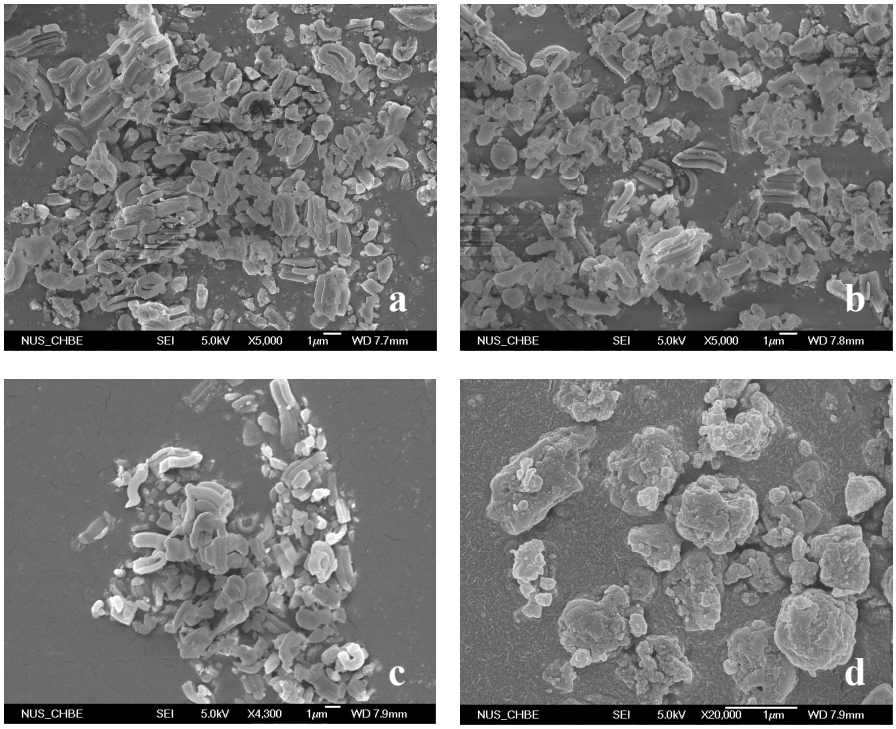

Fig. S4 FESEM images of ES-15: a- before PAA encapsulation and b- after PAA encapsulation and FESEM images of OPS-15: c- before PAA encapsulation and d- after PAA encapsulation.

XPS spectra of materials. XPS was used to characterize the loading of BSA on OPS-15 and encapsulation of OPS-15 with PAA. Fig. S5 shows the N1s XPS spectra of OPS-15, BSA/OPS-15 and PAA-encapsulated BSA/OPS-15. It can be observed that, compared with OPS-15, both BSA/OPS-15 and PAA-encapsulated BSA/OPS-15 samples have a higher N 1s peak located at around 399 eV. Since this N1s peak is attributed to the nitrogen atoms present in the amide bonds in both the polypeptide chain and amino acids, the presence of this intense N 1s peak clearly indicates the entrapment of BSA into SBA-15. Meanwhile, the higher intensity of N1s peak also suggests the higher loading amount of BSA on these two samples

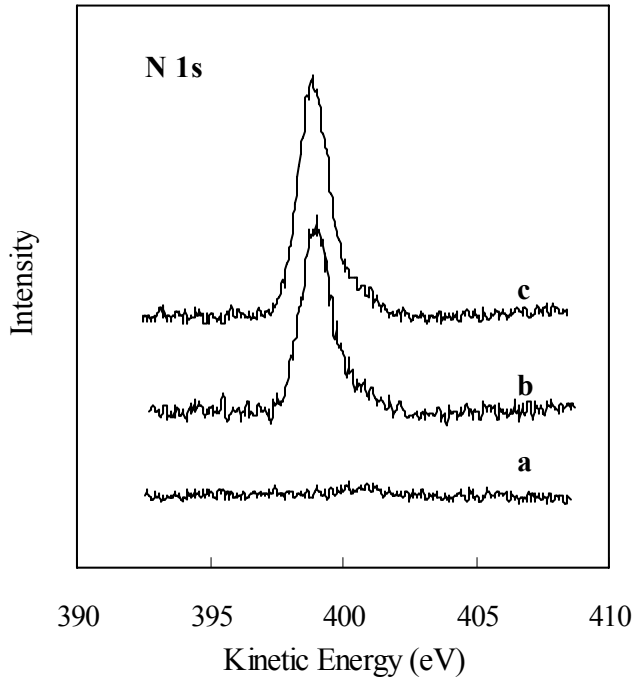

Fig. S5 N1s XPS spectra of: a- OPS-15; b- BSA/OPS-15 and c- PAA-encapsulated BSA/OPS-15.

Fig. S6 shows the C1s XPS spectra of PAA, BSA/OPS-15 and PAA-encapsulated BSA/OPS-15. PAA [Fig. S6(a)] reveals two peaks at 284.6 and 288.6 eV, which are assigned to C-C and O-C=O bonds in PAA chain, respectively. After BSA/OPS-15 has been encapsulated with PAA [Fig. S6(c)], there is a broad O-C=O peak appearing at 288.6 eV, which is attributed to the increase of carboxyl groups on the surface as a result of PAA encapsulation.

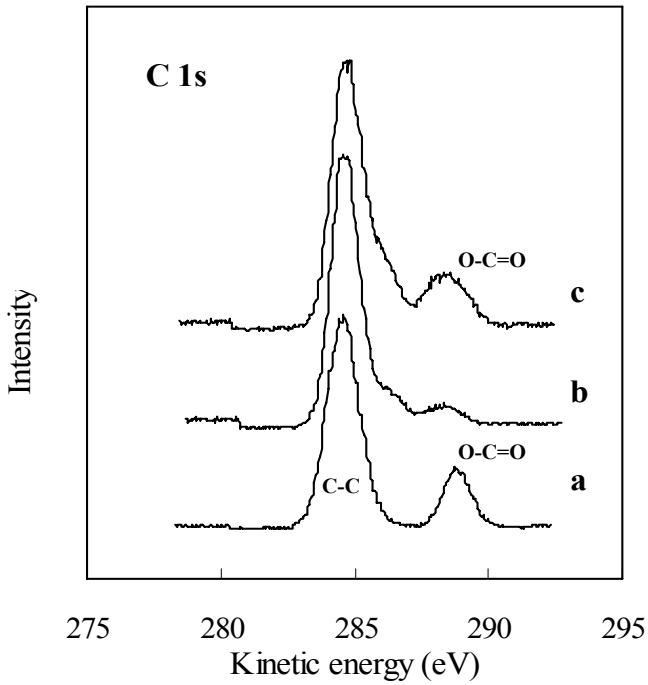

Fig. S6 C 1s XPS spectra of: a- PAA; b- BSA/OPS-15 and c- PAA-encapsulated BSA/OPS-15.

Cytotoxicity studies. Fig. S7 shows the cell viability of S-15, OPS-15 and PAA-encapsulated OPS-15 at two different concentrations of SBA-15. The results show that the cytotoxicity of all three samples increases in relation to the increase of the sample concentration ($p < 0.05$). The results also demonstrate that the effects of the cytotoxicity of OPS-15 and PAA-encapsulated OPS-15 are lower as compared with that of pure SBA-15. The cell viability of OPS-15 and PAA-encapsulated is more than 80% even at a high concentration of 0.5 mg/ml, suggesting that introduction of amine groups could attenuate the cytotoxicity induced by pure silica. Additionally, it is interesting to note that, after 24 hours of incubation with OPS-15, the fibroblasts were found to be more than 100% viable relative to the control cells at the particle concentration of 0.1 mg/ml, indicating that the introduction of amine group on SBA-15 surface could induce the propagation of the fibroblasts. It should be mentioned that for OPS-15, although the template P_{123} cannot be fully removed, it will not increase the risk of the application of SBA-15 as drug matrix. Actually, this kind of amphiphilic copolymers can also be used for drug delivery [6].

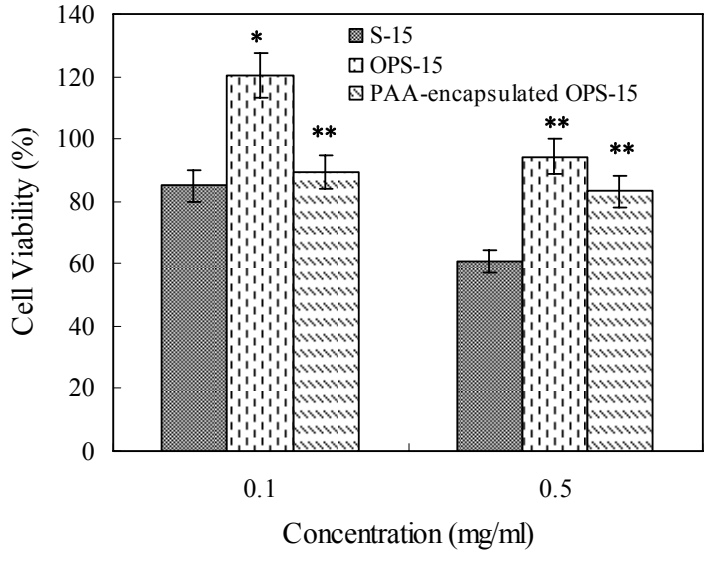

Fig. S7 Cytotoxicity of S-15, OPS-15 and PAA-encapsulated OPS-15 as measured by MTT assay. The results (n=3) are expressed as mean ± SD and the differences between samples were considered significant at $p<0.05$, * $p < 0.01$, ** $p < 0.05$.

pH transition release study. In order to simulate successive pH change in oral administration, the release of BSA from PAA-encapsulated OPS-15 was studied in the acid condition (pH at 1.2) for 4 hours, and the pH was then adjusted to 7.4 ± 0.1 with 1 N sodium hydroxide and monobasic potassium phosphate.

Fig. S8 shows the release profile of BSA from PAA-encapsulated OPS-15 during the transition from pH 1.2 to pH 7.4. It can be seen that BSA is hardly released at pH 1.2 and an increase of pH to 7.4 results in the faster release of BSA. The result clearly not only indicates that BSA has not been irreversibly attached to PAA, but also confirms that BSA can be held at a lower pH of 1.2 and released after the pH has been changed to 7.4.

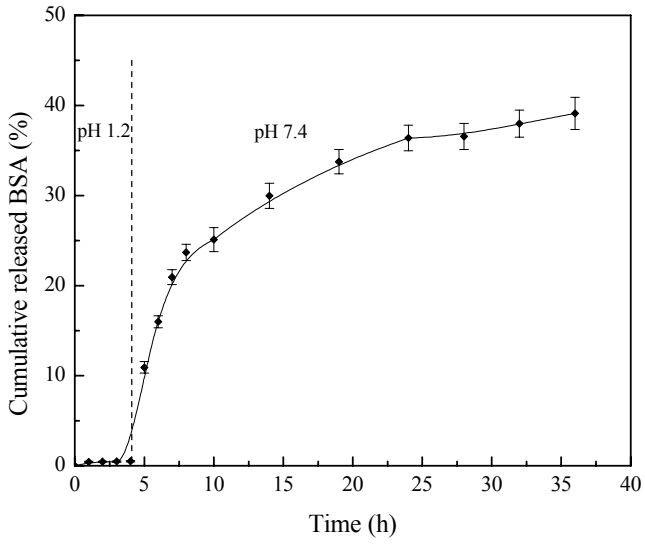

Fig. S8 BSA release profile for pH transition from 1.2 to 7.4

TGA analysis after the release testing. At the end of the release studies, all of the above solid samples were separated from the release media by centrifugation and further drying for TGA analysis to measure the amount of BSA still remaining on the samples. Table S1 summarizes the TGA results of these samples together with the original samples. For amine-functionalized SBA-15 prepared by one-pot synthesis (OPS-15), the weight loss between 100-800ºC is mainly due to the remaining copolymer template, which can not be completely removed by ethanol extraction. It can be seen that the weight loss increased after SBA-15 was loaded with BSA and the resulting BSA/OPS-15 was encapsulated with PAA. It is interesting to note from Table S1 that the weight loss of PAA-encapsulated BSA/SBA-15 (86.6%) after the release test at pH 1.2 is higher than that of other samples (around 50%), indicating that there is more BSA remaining on PAA-encapsulated SBA-15 after the release test at pH 1.2. The TGA results further confirm that BSA could be entrapped inside the mesopores at lower pH conditions.

Table S1 TGA results for SBA-15 samples

Sample	Weight loss (100 - 800ºC, wt %)	Estimated results (wt %)
OPS-15	14.2	
		BSA loading, 20.2
BSA/OPS-15	31.6	
		PAA coating, 6.3
PAA-encapsulated BSA/OPS-15	34.5	
		BSA loading, 16.3
PAA-encapsulated BSA/OPS-15 after the release testing at pH 1.2	29.8	Remaining BSA, 86.6
PAA-encapsulated BSA/OPS-15 after the release testing at pH 7.4	22.6	Remaining BSA, 56.0
Unencapsulated BSA/OPS-15 after the release testing at pH 1.2	22.2	Remaining BSA, 49.4
Unencapsulated BSA/OPS-15 after the release testing at pH 7.4	22.8	Remaining BSA, 45.8

(Note: BSA loading amount can not be directly obtained through the weight loss as shown in TGA results, but estimated by the equation of: (31.6-14.2)/(1-0.316)/[100+(31.6-14.2)/(1-0.316)]. Other estimated results are obtained in the similar way. For OPS-15 samples encapsulated with PAA, BSA weight loss during encapsulation process has been estimated around 2.9%)

Reference:

1. D. Zhao, J. Feng, Q. Huo, N. Melosh, G. H. Fredrickson, B. F. Chmelka and G. D. Stucky, *Science*, 1998, **279**, 548.
2. (a) J. P. Gallas,and J. C. Lavalley, *Langmuir*, 1990, **6**, 1364. (b) J. P. Gallas and J. C. Lavalley, *Langmuir*, 1991, **7**, 1235.
3. K.C. Vrancken, P. van Der Voort, I. Gillis-D'Hamers, E. F. Vansant and P. J. Grobet, *J. Chem. Soc., Faraday Trans.*, 1992, **88**, 3197.
4. E. Gianotti, V. Dellarocca, L. Marchese, G. Martra, S. Colucciaa and T. Maschmeyerc, *Phys. Chem. Chem. Phys.*, 2002, **4**, 6109.
5. R. van Grieken, G. Calleja, G. D. Stucky, J. A. Melero, R. A. García and J. Iglesias, *Langmuir*, 2003, **19**, 3966.
6. A. V. Kabanov and V. Y. Alakhov, in *Amphiphilic block copolymers: self-assembly and applications*, ed. P. Alexandridis and B. Lindman, Elsevier, Amsterdam, 2000, pp. 347-376.